DEVELOPMENT OF GENETICALLY ENCODED HEME SENSORS

A Thesis
Presented to
The Academic Faculty

By

Raven Mariah Harvey

In Partial Fulfillment
Of the Requirements for the Degree
Master of Science in Chemistry

Georgia Institute of Technology

May 2015

DEVELOPMENT OF GENETICALLY ENCODED HEME SENSORS

Approved by:

Dr. Amit R. Reddi, Advisor
School of Chemistry
Georgia Institute of Technology

Dr. Christoph Fahrni
School of Chemistry
Georgia Institute of Technology

Dr. Wendy L. Kelly
School of Chemistry
Georgia Institute of Technology

Date Approved: April 23, 2015

To Justin –
Husband. Friend. Partner in crime.
I can't do me without you.

ACKNOWLEDGEMENTS

TABLE OF CONTENTS

LIST OF TABLES

LIST OF FIGURES

LIST OF ABBREVIATIONS

Abbreviation or Symbol	Term
Aβ	Amyloid-β Protein
AD	Alzheimer's Disease
ALA	δ-Aminolevulinic acid
Cu	Copper
Cyt b_{562}	Cytochrome b_{562}
E. coli	*Escherichia coli*
EV	Empty vector
FP	Fluorescent protein
FRET	Förster resonance energy transfer
FT	Flow through
ER	Endoplasmic reticulum
GFP	Green fluorescent protein
Hb	Hemoglobin
HD	Huntington's Disease
hem1Δ	Yeast without hem1 encoding ALA synthase
his_6-tag	Hexahistidine tag
HS1	Heme sensor 1
HS1-monoHis	Heme sensor 1 with Met7Ala mutation
IPTG	Isopropyl β-D-thiogalactopyranoside
IR	Infrared
Leu	Leucine

Mb	Myoglobin
MBP	Maltose binding protein
min	Minute
mL	Milliliter
nm	Nanometer
nM	Nanomolar
NFT	Neurofibrillary tangles
Ni column	Nickel affinity column
NPAS2	Neuronal PAS domain 2
OD	Optical density
PBS	Phosphate-buffered saline
PD	Parkinson's Disease
pI	Isoelectric point
PROS	Partially reduced oxygen species
ROS	Reactive oxygen species
SC	Synthetic complete medium
SCE	Synthetic complete medium supplemented with ergosterol and tween-80
SDS-PAGE	Sodium dodecyl sulfate polyacrylamide gel electrophoresis
SThM	Scanning thermal microscopy
Succinyl-CoA	Succinyl-coenzyme A
TEV	TEV protease
μg	Microgram

μL	Microliter
μM	Micromolar
UV-Vis	Ultraviolet-visible
WT	Wild type
Yeast	*Saccharomyces cerevisiae*

SUMMARY

Due to the biological importance of heme and its implication in various disease states, uncovering how it is transported throughout the cell is of vital importance. Some of the strongest *in vivo* tools present in the literature are FRET-based sensors using a number of chromophores that are optimized and expanded from GFP. In order to elucidate the movement of heme throughout the cell, GFP FRET-based heme sensors were designed, expressed, and purified to be further characterized *in vitro*. This series of heme sensors were expressed in *Saccharomyces cerevisiae* to monitor the *in vivo* movement of heme. Different growth conditions were explored to monitor the effect of these changes to cytosolic heme availability. These heme sensors are now poised to address the movement of heme from the mitochondria to other targets in the cell under a variety of conditions. This will provide insight into heme trafficking pathways, as well as the role heme plays in neurodegenerative diseases and aging.

CHAPTER 1

INTRODUCTION

1.1 Heme Biology

Heme is an essential but cytotoxic iron-containing protein cofactor and signaling molecule. While its biosynthesis and degradation are well understood, little is known about the transport and trafficking of heme. Knowledge of the latter will have a tremendous impact on understanding how cells assimilate heme into metabolism while also mitigating its inherent cytotoxicity. Our approach toward studying heme homeostasis is to couple intracellular heme imaging with genetic screens to identify genes that, when overexpressed or deleted, will alter the distribution of heme. Towards this end, we describe the design and characterization of the first genetically encoded ratiometric heme sensors, which will be used in future studies to study heme trafficking and signaling.

Heme is an iron-containing porphyrin that can adopt several different oxidation states and take on a variety of structures. The most biologically abundant variant of heme, heme *b*, is used as a cofactor for a wide range of proteins, including peroxidases,[1] and contains two vinyl, two propionate, and four methyl side chains. The coordinated iron atom within the porphyrin ring can either adopt a ferric (Fe^{3+}) or ferrous (Fe^{2+}) oxidation state. The other common variants of heme, heme *a* and heme *c*, are used as cofactors for the enzyme cytochrome *c* oxidase[2] and as a covalently attached cofactor in c-type hemoproteins[3], respectively.

Heme is synthesized in the mitochondria through a highly conserved eight-step process known as the Shemin pathway.[4] This process begins with the condensation of

1

glycine and succinyl-coenzyme A (succinyl-CoA) to give the first intermediate δ-aminolevulinic acid (ALA) and ends with Fe^{2+} insertion into protoporphyrin IX to produce heme (iron protoporphyrin IX). Heme is then redistributed to multiple organelles in a number of locations across the cell including the mitochondrial intermembrane space, cytosol, endoplasmic reticulum (ER), and nucleus to perform its numerous functions.

1.2 Functions of Heme

Cellular functions of heme include chemical catalysis[5], electron transfer[6], gas binding and transport[7], and involvement in various signaling pathways[8]. Recently, it has been found that heme catalyzes an increase in peroxidase activity and the reduction potentials increase in the relevant redox intermediates when heme covalently binds to a heme peroxidase[1]. Heme is utilized as a prosthetic group in cytochrome *c,* and facilitates electron transfer between Complex III and Complex IV in the electron transport chain[3]. Due to the high reactivity of the iron center in heme, cytochrome *c* is shown to fully envelop its substrate in order to efficiently and selectively transport electrons and to avoid adverse redox reactions[9]. The demand for molecular oxygen in various roles throughout biology necessitates its transport through the organism at the cellular level, as well as at the systems level. Two of the most studied oxygen binding and transport molecules, myoglobin (Mb) and hemoglobin (Hb), utilize heme as their prosthetic group allowing for the binding and transport of oxygen in muscle tissues and blood, respectively.[10] Heme is also implicated in a number of sensing pathways including cellular oxygen sensing through activation of the transcription factor Neuronal PAS

domain 2 (NPAS2) when heme is bound to the PAS domain.[7] As an effector molecule, heme is found to regulate gene expression in yeast.[11]

As seen above, heme performs various functions in every cellular compartment including chemical catalysis of peroxidases in the endoplasmic reticulum peroxidases, acting as a cofactor across complexes in the respiratory pathway in the mitochondria, and in the activation of transcription factors in the nucleus. Its transport to these different compartments is largely unknown, calling for a reliable method to visualize the movement of heme *in vivo*.

1.3 Cytotoxic Effects of Free Heme

Despite its essentiality, heme is cytotoxic due to its ability to induce oxidative stress[12] and to interact with membranes[13]. Indeed, free heme can aid in the production of reactive oxygen species (ROS). ROS are highly reactive in the cellular environment and include the compounds superoxide anion (O_2^-) and hydroxyl radical ($^{\cdot}OH$). These ROS have been implicated in the damage of DNA, lipids, and proteins.[12] Heme is lipophilic and, when its biosynthesis, trafficking, and degradation is misregulated, can lead to heme aggregation at the membrane resulting in oxidation, leading to an increase in permeability and a variety of membrane disorders.[13]

A number of pathologies including Alzheimer's Disease (AD), Parkinson's Disease (PD), and Huntington's Disease (HD) have been shown to have a misregulation of heme that leads to, or happens concurrently with, their disease state[12]. AD is the most common age-related neurodegenerative disease that is characterized by the accumulation of insoluble extracellular amyloid-β protein (Aβ) plaques in the synaptic gap, as well as

the formation of neurofibrillary tangles (NFTs) in neurons – caused by the aggregation of hyperphosphorylated Tau protein.[14] Heme and copper (Cu) have been found to bind Aβ peptides together, as seen in Figure 1, and produce a large number of partially-reduced oxygen species (PROS) like H_2O_2, implying the potential for heme-Cu-Aβ complexes to contribute toxicity to the AD pathology.[15] When heme is mistrafficked there is an increase in free heme, which can then bind to Aβ to perpetuate AD toxicity. PD is a
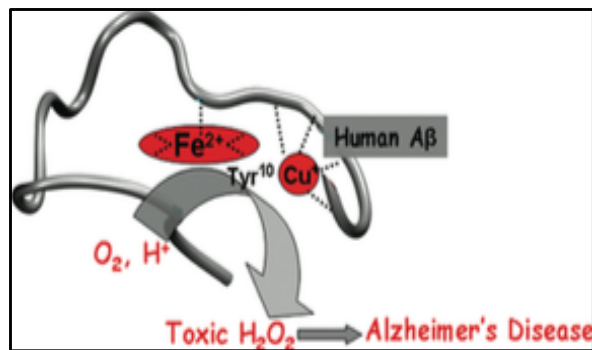
Figure 1. Heme-Cu complex that binds the Aβ peptide in Alzheimer's Disease. The iron center can catalyze the production of toxic H_2O_2. This figure was taken from Pramanik et al. (2011) as Abstract Figure.[15]

neurodegenerative disorder that is characterized by the loss of dopaminergic neurons in the *substantia nigra* and the deposition of intracellular Lewy bodies.[12] While there is not a clear picture of how or when this happens, iron levels are shown to be increased in the *substantia nigra* which could lead to the production of ROS and lipid peroxidation.[12] Since heme is a cellular source of iron upon its degradation, its premature degradation could lead to the increase in iron shown in the PD pathology. The same is true in the HD

pathology, which shows increased iron levels during the early stage and a continued

increase in iron levels as the disease progresses[12]. This could be indicative that iron plays

a role in the progression of the disease.
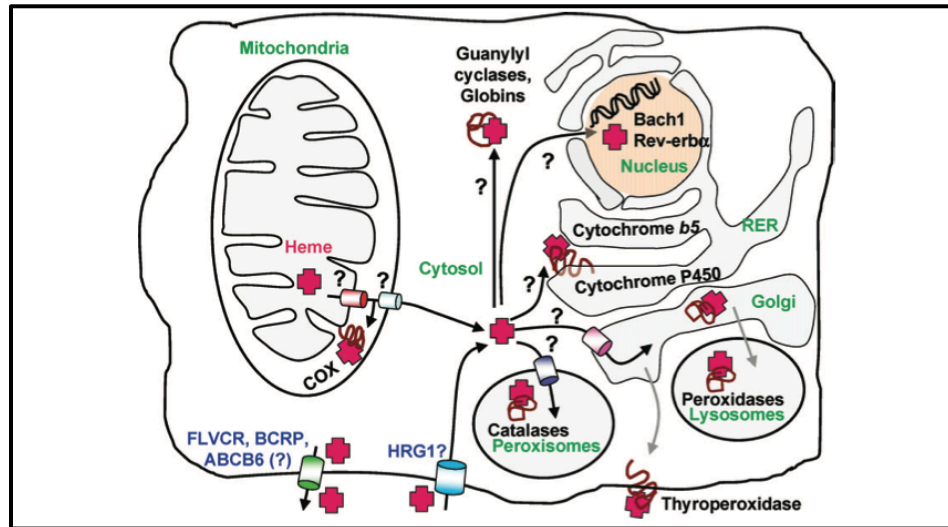
Figure 2. Current model proposed for heme transport throughout the cell. Heme (red
cross) is synthesized in the mitochondria but the possible pathways it takes to reach all
cellular targets like the rough endoplasmic reticulum (RER) are unknown (illustrated
with black arrows and question marks)[3]. This figure was taken from Severance and
Hamza (2009), as Figure 2.

Recognizing that heme is biosynthesized in the mitochondria, that heme performs

diverse roles previously discussed in almost all organelles of the cell, and that free heme

has been shown to be incredibly cytotoxic, it would stand to reason that there is a well-

developed system to closely regulate the trafficking of heme from the mitochondria to its

various targets to avoid adverse effects. As illustrated in Figure 2, heme is used in almost

all organelles of the cell. There are two main hypotheses as to how heme is transported to

perform its numerous functions across the cell.[3] The first is a chaperone independent

process in which the presence of a labile heme (shown by the red cross) pool in the

cytosol that can be activated in response to a stimulus and then shuttled to different

organelles[3]. The second hypothesis is a chaperone dependent process where heme is more

tightly regulated and transported to its destinations by heme chaperones upon production

in the mitochondria[3]. This hypothesis is largely favored due to the catastrophic effects

labile heme can have in the cell. Currently, the means by which heme is transported

throughout the cell is largely unknown, calling for a way to visualize heme in order to

better understand heme biology and how its misregulation may play a role in a number of

pathologies.

1.4 Current Methods of Heme Detection

Currently, there are no methods that can image labile heme and how it moves

throughout intact cells. Heme exhibits rich electronic and vibrational spectra that can be

used to find its concentration and coordination environments. These properties are largely

utilized in techniques such as Ultraviolet-visible (UV-Vis) spectroscopy, Resonance

Raman, and photothermal microspectroscopy. UV-Vis spectroscopy measures the

characteristic absorption of heme and can yield concentrations, coordination states, and

other electronic properties. This method falls short in its relative insensitivity when

compared to other methods such as fluorescence spectroscopy. Resonance Raman

spectroscopy utilizes a laser that excites a molecule within its electronic absorbance band

to produce large Raman enhancements for the vibrational modes of the molecule[16]. This

method can visualize structural changes in heme that can be related to oxygen binding

and transport in the hemoproteins Mb and Hb, as well as electron transfer along the electron transport chain[16]. While Raman microscopy is able to spatially resolve heme pools, it largely reports on the most abundant hemoproteins, which have inert populations of heme, thus still leaving us unable to visualize the movement of labile heme. Photothermal microspectroscopy is derived from two parent techniques, infrared (IR) spectroscopy and scanning thermal microscopy (SThM). Photothermal microspectroscopy is able to spatially resolve spectroscopic properties to a scale of about 20-30 nm. This technique is very useful in determining which oxidation state heme is in when it's used as a cofactor for various enzymes and macromolecules, but still falls short in its ability to monitor labile heme pools in intact cells[17].

In an effort to increase sensitivity, fluorescent heme analogs have been implemented as tracers to monitor heme transport in intact cells[18]. While the sensitivity and ability to visualize heme movement is largely improved in this method, the major drawback is that these analogs are chemically different from heme and can dramatically alter the fundamental coordination chemistry of the metalloporphyrin. This becomes an issue in trying to elucidate various heme transport and trafficking pathways because these variants can give rise to their own distinct trafficking and transport schemes, skewing the visualization of the natural pathways heme takes throughout the cell. Due to the drawbacks of the aforementioned methods, a new method must be devised in order to monitor natural heme movement in cells without perturbing the endogenous pathways to gain a clear understanding of how heme is transported throughout cells. If successful, this method could be paired with other methods, like genetic screens, to fully uncover the

heme biology of different organisms and to better understand what effects, if any, heme is having in the progression of several disease states.

The development of fluorescent reporters for transition metals has greatly aided in understanding the functions of metals in biology. Small molecule fluorescent probes have been developed and used *in vivo* to report on the level of the target transition metal, but they struggle with toxicity and solubility[19,20]. Many small molecule fluorescent sensors also have difficulty reaching a high enough affinity to monitor transition metal levels in extremely low concentrations in a cellular environment[21]. To resolve this issue, genetically encoded fluorescent protein-based sensors have been developed. Green Fluorescent Protein (GFP) was isolated from the jellyfish *Aequorea victoria* in 1961[22] and further optimized to gain increased brightness as well as expand the library of colors emitted to increase use in cells[23]. One of the major benefits of using fluorescent proteins (FPs) is the ability to control their localization, as well as pairing them with other FPs for ratiometric imaging via Förster Resonance Energy Transfer (FRET).[24] FRET has been utilized to sense multiple analytes, including metals like zinc and copper. For example, Dittmer et al. (2009) used these FRET sensors to visualize the subcellular localization of zinc in living cells. They utilized a zinc-binding domain that resulted in a conformational change upon zinc binding, bringing the two chromophores close enough for FRET to occur[25]. These FRET sensors were then further developed to simultaneously monitor zinc uptake into different subcellular compartments. To accomplish this, two FRET pairs, green-red and cyan-yellow, were used concurrently to monitor zinc uptake in different compartments including the nucleus, ER, Golgi, and mitochondria[26]. As seen in Figure 3, these two FRET pairs were imaged while being colocalized in the same set of cells.
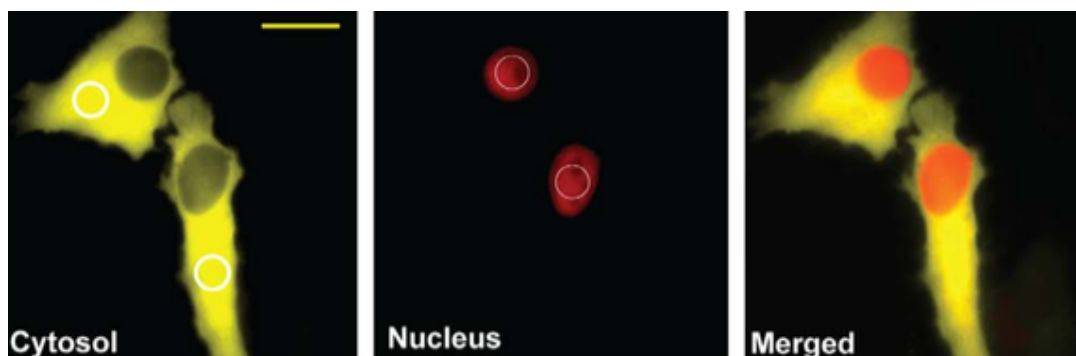
Figure 3. Colocalization of two FRET pairs. The Cyan-Yellow FRET pair was targeted to the yeast cytosol (left panel) to show cytosolic zinc concentrations. The Green-Red FRET pair was targeted to the yeast nucleus (middle panel) to show nuclear zinc concentrations. The overlay of these two images shows their utility within the same cells simultaneously. This figure was taken from Miranda et al. (2012), as Figure 4c.[26]

These powerful tools can be used to monitor the movement of metals and small molecules in living cells under a multitude of conditions. The strength of FRET lies in the ability to design sensors with high specificity for different ligands, subcellular targeting, and the plethora of FPs that have been created to cover the entire visible range, into near-IR and near-UV as well.

Due to the success of previous FRET-based sensors for the in vivo monitoring of various analytes, the same approach toward the study of heme will significantly aid in better understanding its cell biology, including its transport, trafficking, and role in signaling. Herein, I report the design, purification, and initial *in vivo* characterization of a novel heme-dependent ratiometric FRET sensor.

CHAPTER 2

DESIGN AND PURIFICATION OF HEME SENSORS

2.1 Introduction

Our heme-dependent FRET sensor, Heme Sensor 1 (HS1), was designed as a tridomain sensor including a heme-dependent FRET donor, eGFP, that is fused to the heme-binding region cytochrome b_{562} (cyt b_{562})[27], which acts as the FRET acceptor, and a heme-insensitive chromophore, mKATE2.

Figure 4. HS1 ribbon model depicting the FRET donor, eGFP, cyt b_{562}, which binds the FRET acceptor, heme, and the heme- and eGFP-insensitive chromophore, mKATE2[27].
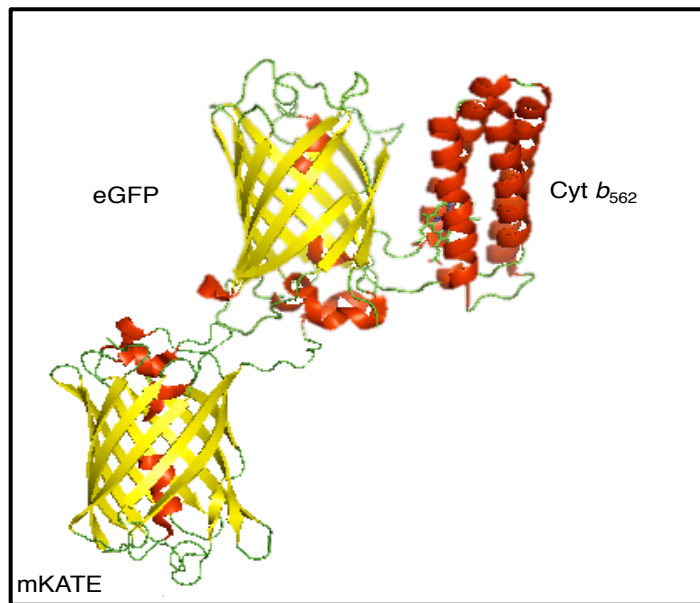
FRET is an extremely useful tool that takes advantage of the dipole-dipole interactions resulting from overlap between the excited state of one chromophore (donor) and the ground state of another chromophore (acceptor). The efficiency of FRET is highly dependent upon distance between and orientation of two chromophores[28]. These qualities make FRET pairs very useful in monitoring a ligand binding event if a conformational change takes place upon binding, bringing the donor and acceptor closer together, resulting in a change in fluorescence. FRET is sensitive to changes with the relation $1/r^6$ with r being the distance between chromophores[28]. The acceptor molecule, heme, can accept the excited-state energy from the donor molecule, eGFP, when they are brought in close proximity to each other. To accomplish this, the heme binding domain cyt b_{562} was fused to eGFP, bringing the heme close enough to eGFP for FRET to occur. Cyt b_{562} is an *Escherichia coli (E. coli)* electron transport protein that binds heme using a His/Met coordination, Met7 and His102.[29,30]

While heme does not fluoresce, it can accept energy between 400-600 nm, which overlaps with the fluorescence emission of eGFP between 510-530 nm. Due to this overlap, if heme can be positioned near the eGFP chromophore, it will accept the excited state energy from eGFP, thereby quenching fluorescence. In order to maximize this effect, Arpino et al. (2012) tested the insertion of cyt b_{562} into eGFP to optimize the quenching of eGFP fluorescence upon heme binding[27]. This was accomplished by utilizing the nonhomologous recombination method, transposon mutagenesis, which involves creating a library in which cyt b_{562} was randomly inserted into eGFP, and then screened for mutants that retained full eGFP fluorescence. The mutants that did exhibit undisturbed fluorescence after cyt b_{562} insertion were then sequenced, and mutants that

11

showed correct sequences were screened for their ability to be fully quenched upon heme binding. Three mutants were chosen that retained full excitation of eGFP at 488 nm and were fully quenched by heme binding. These mutants, CG2, CG4, and CG6, were found to all be quenched to the same degree upon heme binding, but CG6 had behavior mirroring that of native cyt b_{562} in that it had a similar K_D value for heme. CG2 and CG4 were found to require 7.5- and 3-fold greater concentration of heme, respectively, in order to achieve full quenching of the eGFP chromophore. For this reason, CG6 was obtained from Arpino et al. (2012) and was chosen as the ideal two-domain scaffold on which to build our sensor.

To be confident that the fluorescence quenching observed is due to heme binding, and not an indirect event that is modifying or denaturing the chromophore, an internal standard that accounts for inherent fluctuations in fluorescence is necessary. To address this, we fused another chromophore, mKATE2, to CG6 via a Gly-Ser linker. mKATE2 (excitation: 588 nm, emission: 633 nm) is largely insensitive to energy transfer from eGFP (excitation: 488 nm, emission: 510 nm) and heme[31]. This chromophore is beneficial as an internal standard because its fluorescence will not change in the presence of heme, but it will indicate if the cellular environment is prematurely degrading the chromophores. By utilizing CG6 and mKATE2, we have designed a ratiometric heme sensor that will change with varying concentrations of heme. The fluorescence ratio of eGFP to mKATE2 will change as heme availability fluctuates. An increase in heme binding will result in a decrease in eGFP fluorescence and no change to the mKATE fluorescence emission, thus lowering the eGFP:mKATE2 fluorescence ratio.

To purify HS1, a number of methods were tested until pure protein was isolated. The first step was to fuse a hexahistidine tag (his$_6$-tag) to the N-terminus of the protein. We utilized the his$_6$-tagged HS1 on a nickel affinity column (Ni column) to separate HS1 from other proteins present in the crude lysate. Due to histidine's ability to bind heme, it was then imperative to remove the his$_6$-tag from HS1 so that it would not skew binding affinities and heme concentrations[32]. To do this, a thrombin site was added to allow selective cleavage of the his$_6$-tag from HS1. The use of thrombin proved difficult due to precipitation of HS1 upon cleavage attempts. To overcome this, a TEV protease cleavage site was then added to HS1 between the his$_6$-tag and the N-terminus of mKATE2. TEV, a cysteine protease, has been shown to be highly selective and widely used in protein purification for the cleavage of his$_6$-tags[33]. The TEV that was used in this purification also had a his$_6$-tag engineered onto it so that following cleavage, the his$_6$-tag from HS1, as well as the TEV protease, would bind to the Ni column while HS1 eluted.
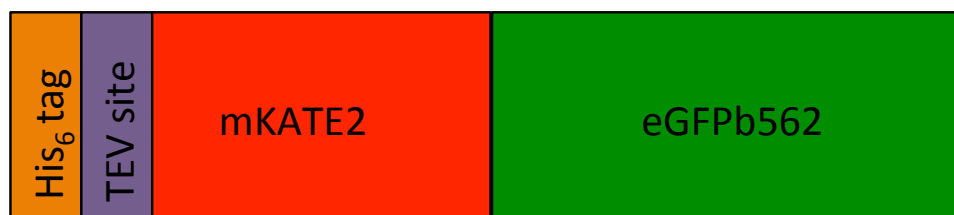

Figure 5. Linear, cartoon design of HS1 including the his$_6$-tag and the TEV cleavage site for purification methods.

2.2 Purification of HS1

Purification of this protein began with cloning CG6 into pET30a(+), which already had a his$_6$-tag at the N-terminus, via *Bam*HI and *Hind*III restriction sites. mKATE2 was then fused to the N-terminus of CG6 via a *Bam*HI restriction site linker, for expression in *E. coli* BL21(DE3). Initially, the success of the TEV digest was unclear due to the relatively small change in molecular weight before and after cleavage of the his$_6$-tag (0.82 kDa), unable to be reliably resolved by Sodium Dodecyl Sulfate Polyacrylamide Gel Electrophoresis (SDS-PAGE). For this reason, Maltose-Binding Protein (MBP) was fused to the N-terminus of mKATE2. As MBP is a 42.5 kDa protein, it adds the mass necessary to visualize TEV cleavage by SDS-PAGE[34]. This modification was highly useful in determining the efficiency of the his$_6$-TEV protease, but created more problems in the purification route. After the addition of MBP, the expression of HS1 fluorescence was adversely affected, resulting in an overall loss in protein color, a decrease in chromophore absorbance and fluorescence, and a loss in efficient separations on the Ni column. This modification was discarded due to the problems it created, but was useful in initially detecting the cleavage efficacy of the modified his$_6$-TEV protease.

We returned to the original design of HS1, sans MBP, and continued on with the purification route. Upon cell lysis, the cell-free extract was applied to a Ni column was run to separate his$_6$-HS1 from other proteins present in the cell lysate. Imidazole was used to selectively outcompete the his$_6$-tag on the Ni column upon an increase in imidazole concentration. After elution of HS1, as seen visually by the pink color of the protein, SDS-PAGE was performed to confirm the relative purity of HS1 compared to that of the crude lysate. As seen in Figure 6, the crude lysate showed a multitude of

proteins that largely eluted in the flow through (FT), indicating a lack of interaction with the nickel on the column.
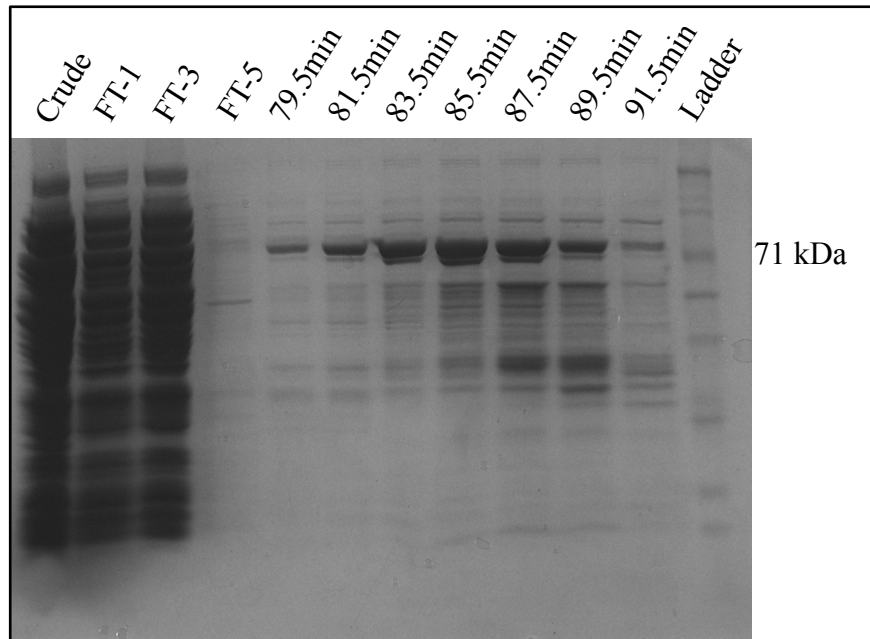
Figure 6. SDS-PAGE confirming efficiency of Ni column for HS1 (65 kDa) purification. Lane 1: HS1 crude lysate. Lanes 2-4: HS1 flow through in low imidazole wash. Lanes 5-11: HS1 elution from various minutes (min) throughout the gradient elution. Lane 12: molecular weight ladder.

The other wells on the gel show samples from 79.5 minutes to 91.5 minutes, during the gradient increase in elution buffer. At 65 kDa, HS1 runs close to the 71 kDa marker. It was consistently seen to run slightly above the molecular weight marker but the band was confirmed as HS1 via MALDI-MS. The HS1 was also found to run in a duplicate state, as indicated by the presence of two bands close together, which could be due to two conformers present after denaturing the protein prior to loading the gel. This hypothesis

was confirmed by running a sample of relative purity on the HPLC and seeing only one peak where HS1 eluted. In order to better understand and confirm this phenomenon, samples could be differentially denatured to see if the population of the two bands increase or decrease. Three samples, 79.5 min, 81.5 min, and 83.5 min were combined and dialyzed against TEV cleavage buffer to remove imidazole.

After dialysis was complete, the his_6-HS1 sample was digested with TEV to cleave the his_6-tag. A sample of HS1 without TEV was also left at room temperature with the TEV cut sample in order to have a control to run on the Ni column that had not been exposed to TEV. The HS1+TEV sample was run on the Ni column and HS1 eluted in the flow through, as indicated by the elution of the pink-colored protein. Once the column was re-equilibrated in equilibration buffer (10 mM Tris, 100 mM NaCl, pH 8, 20 mM imidazole), the HS1+buffer control was run on the Ni column and HS1 was shown to stick to the column until it was eluted with elution buffer (10 mM Tris, 100 mM NaCl, pH 8, 300 mM imidazole), confirming the presence of an intact his_6-HS1. In order to confirm the purity of HS1, and the lack of the TEV protease, SDS-PAGE was performed with various samples after elution of the HS1+TEV sample. As seen in Figure 7, a large
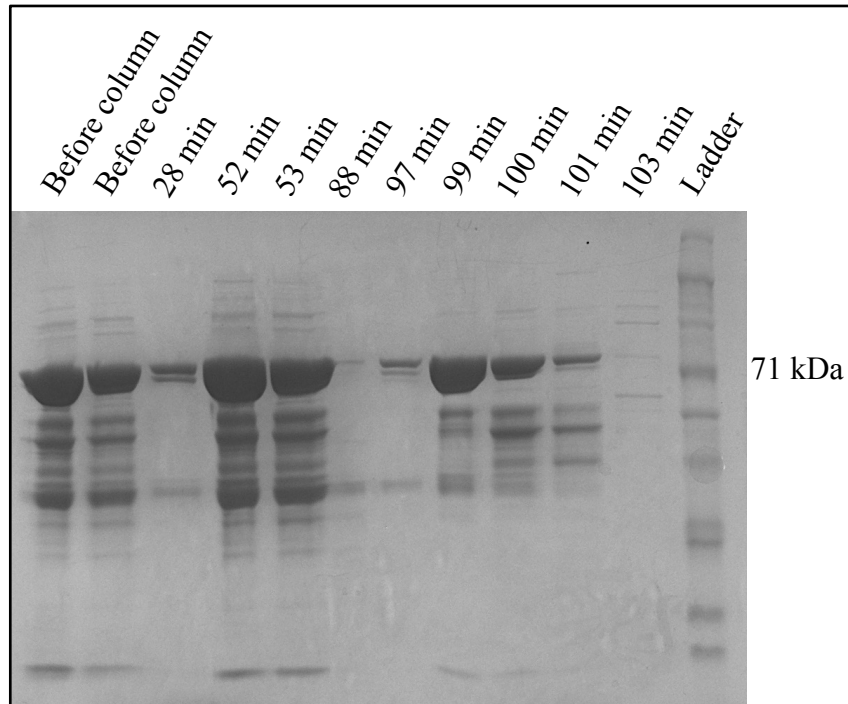
Figure 7. SDS-PAGE after TEV digest and Ni column to obtain HS1 (65 kDa) without the his$_6$-tag. Lanes 1-2: HS1+TEV before running on Ni column. Lanes 3-11: HS1 elution from various minutes (min) throughout the low imidazole elution. Lane 12: molecular weight marker.

amount of impurities were shown to co-elute with HS1. However, the TEV protease was

largely removed from the samples due to the his$_6$-TEV interacting with the Ni column. In

order to obtain pure HS1, ion exchange chromatography was performed to selectively

elute HS1. With a calculated isoelectric point (pI) of 6.59, a cationic column was utilized

to selectively isolate HS1 based on size and amino acid content. To increase the

likelihood of finding pure samples, smaller fractions were collected and checked via

SDS-PAGE. As seen in Figure 8, pure HS1 was successfully isolated.
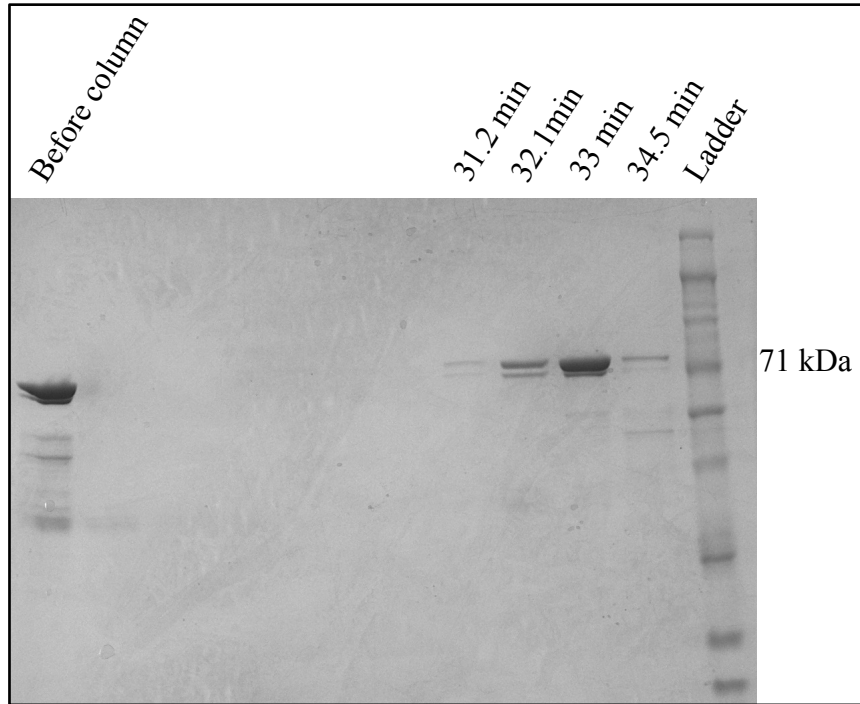
Figure 8. SDS-PAGE confirming HS1 (65 kDa) purity after ion exchange chromatography. Lane 1: HS1 sample before ion exchange chromatography. Lanes 2-7: empty wells. Lanes 8-11: HS1 elution from various minutes (min) throughout the gradient elution. Lane 12: molecular weight ladder.

All of the HS1 samples that demonstrated protein purity were combined, concentrated via spin concentration, and were stored at 4 °C to be used in further experiments.

2.3 Creating a Library of HS1 Mutants

Since HS1 was typically 95% bound with heme, a different sensor was needed to better monitor changes in heme concentrations. It is important to create a sensor that is neither over-saturated or under-saturated so that the sensor can reliably monitor both increases and decreases in heme concentrations. To develop this ratiometric sensor that

would bind heme with a different affinity, a cyt b_{562} Met7Ala mutation was prepared. We hypothesized this mutant to give a weaker binding sensor due to the disruption of the coordination environment. HS1 was shown to be fully quenched in wild type (WT) cells, so it would not be a good tool to monitor an increase of heme. For this reason, HS1-monoHis was cloned and purified.

Following very closely with the HS1 purification, HS1-monoHis was transformed into the expression strain *E. coli* BL21(DE3) to overexpress the mutant proteins. After cell lysis, the 20 mL Ni column was then used to purify the crude HS1-monoHis, and the fractions found to contain the protein were dialyzed to remove imidazole. As seen in Figure 9, HS1-monoHis eluted with the presence of several impurities, but most of the other proteins shown in the crude lysate came out in the flow through.

Figure 9. SDS-PAGE confirming efficiency of Ni column for HS1-monoHis (65 kDa) purification. Lane 1: HS1-monoHis crude lysate. Lane 2: HS1-monoHis flow through in low imidazole wash. Lanes 3-9: HS1-monoHis elution from various minutes (min) throughout the gradient elution. Lane 10: molecular weight ladder.

Samples 73 min, 75 min, and 77 min were combined and dialyzed to remove imidazole. Following dialysis, a digest was performed using a 1:1 molar ratio of HS1-monoHis:TEV over 18 hours. A second nickel affinity column was run to separate the HS1-monoHis from the his$_6$-tag and TEV protease. This protein also showed other impurities present after the second Ni column, necessitating a run on the ion exchange column. After fractions were collected from the ion exchange column, they were checked via SDS-PAGE for purity. As seen in Figure 10, HS1-monoHis was successfully purified and samples of similar purity were pooled and stored at 4 °C for future experiments.

Figure 10. SDS-PAGE confirming HS1-monoHis (65 kDa) purity after ion exchange chromatography. Lane 1: molecular weight ladder. Lane 2: HS1 sample before ion exchange chromatography. Lanes 3-12: HS1 elution from various minutes (min) throughout the gradient elution.

To account for the possibilities of heme non-specifically binding to either chromophore, a mutant of HS1 was made that had the heme-binding region, cyt b_{562}, removed, creating an mKATE2-eGFP Fusion protein. The purification of this control differs in its protease cleavage site from the two previous samples in that it retained a thrombin site instead of a TEV site. This was due to success in earlier purification of an eGFP clone using thrombin and the ease of cloning mKATE2 into that existing clone. The Fusion plasmid was transformed into *E. coli* BL21(DE3). After cell lysis, the 20 mL Ni column was then used to purify the crude Fusion and the fractions found to contain the protein were dialyzed to remove imidazole. As seen in Figure 11, the Fusion protein

21

eluted with the presence of several impurities, but most of the proteins shown in the crude lysate came out in the flow through. Samples 70 min, 72 min, 74 min, 76 min, and 78 min were combined and dialyzed to remove imidazole. Following dialysis,
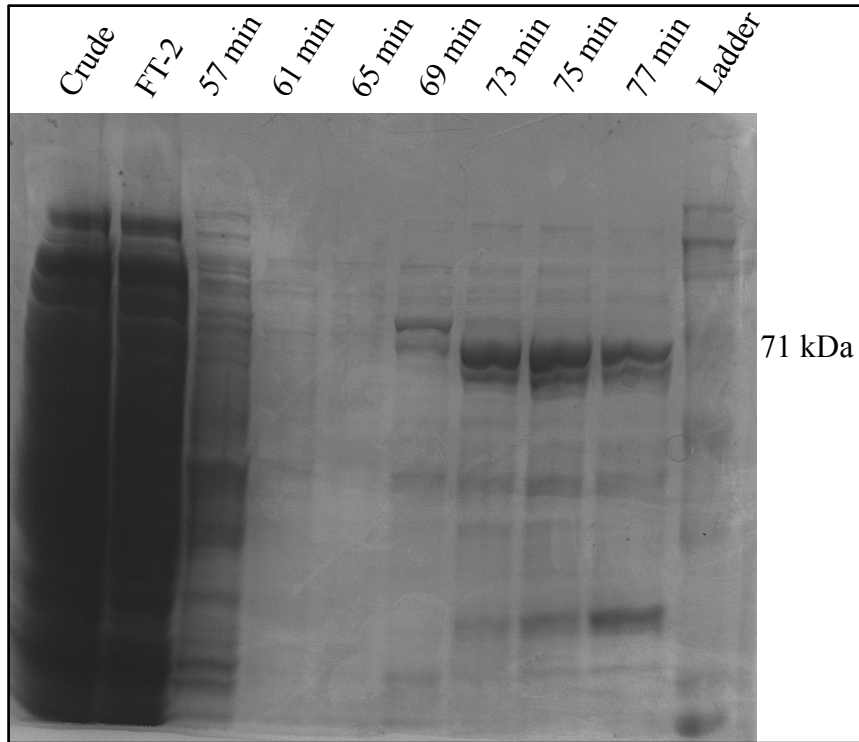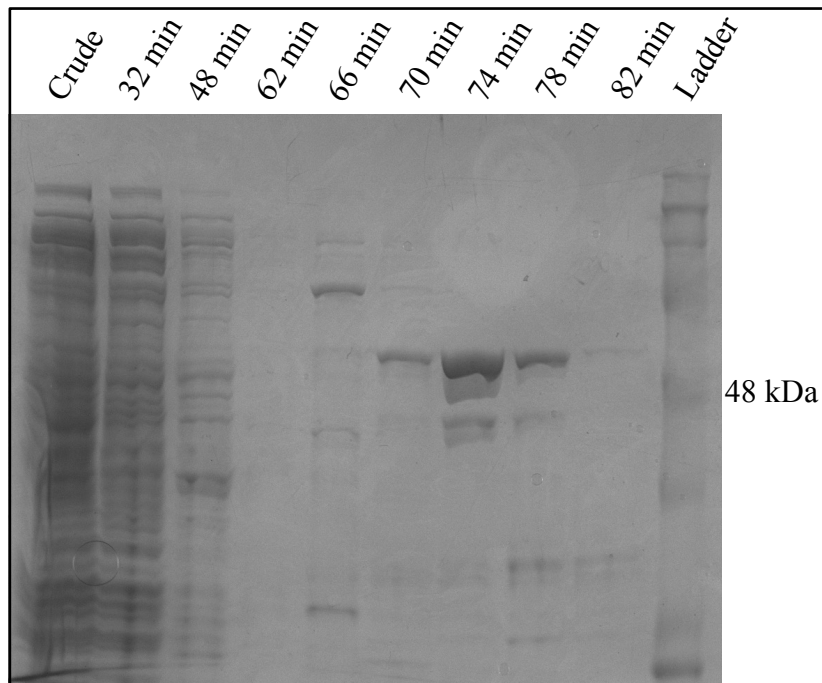

Figure 11. SDS-PAGE confirming efficiency of Ni column for mKATE-eGFP fusion (53.25 kDa) purification. Lane 1: mKATE2-eGFP fusion sample before Ni column. Lanes 2-9: mKATE-eGFP fusion elution from various minutes (min) throughout the gradient elution. Lane 10: molecular weight ladder.

a 1:10 dilution of thrombin (stock concentration of 50 untils/µL) was added to the Fusion sample and a digest was performed over 15 hours. A second Ni column was run to separate the Fusion from the his$_6$-tag and thrombin. This protein also showed impurities after the second Ni column, necessitating a run on the ion exchange column. After

fractions were collected from the ion exchange column, they were checked for purity via SDS-PAGE. As seen in Figure 12, fusion was successfully purified and samples of similar purity were pooled and stored at 4 °C for future experiments.

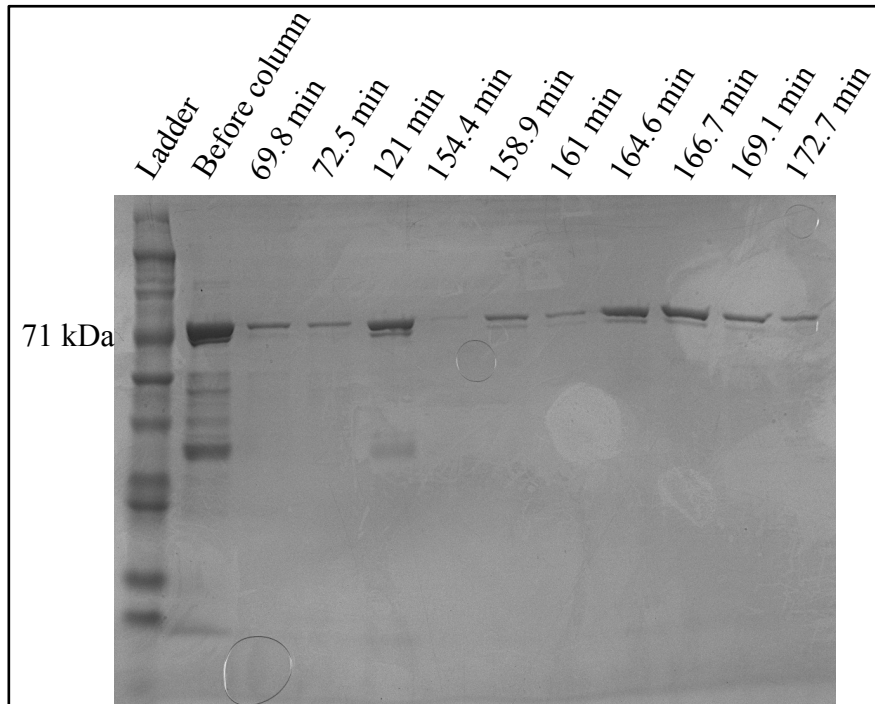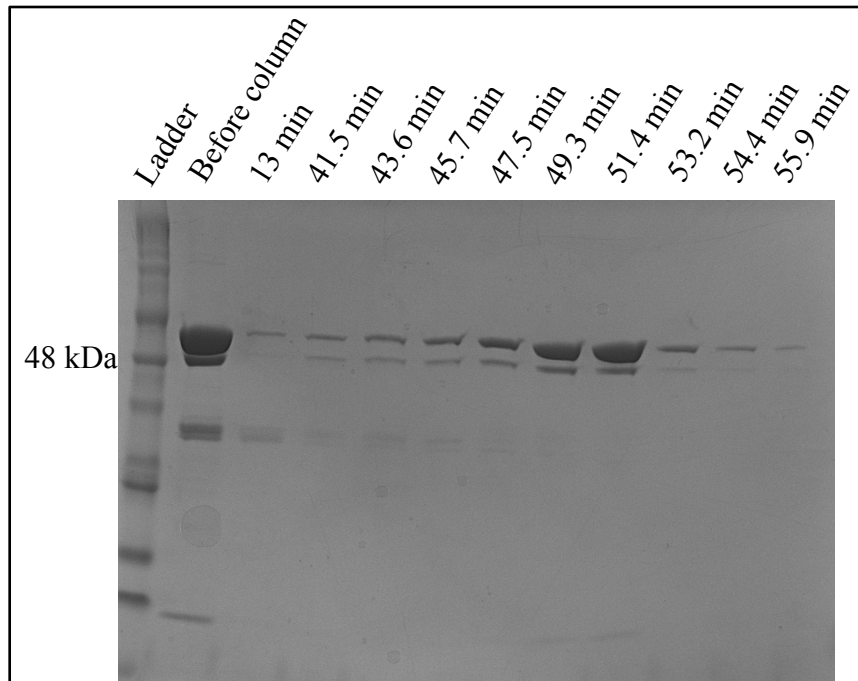**Figure 12.** SDS-PAGE confirming mKATE2-eGFP fusion (53.25 kDa) purity after ion exchange chromatography. Lane 1: molecular weight ladder. Lane 2: mKATE2-eGFP fusion before ion exchange chromatography. Lanes 3-12: mKATE2-eGFP fusion elution from various minutes (min) throughout the gradient elution.

2.4 Determination of Cellular HS1-monoHis Concentration

An important aspect of creating a robust *in vivo* sensor is to ensure its presence does not perturb the natural biology of the analyte that is being monitored. In order to find a reliable method to quantify HS1-monoHis sensor levels in the yeast cell, two

different methods were employed to determine the ease and accuracy of each method. Both methods included creating a calibration curve with purified HS1-monoHis protein and testing the sensor concentrations of HS1-monoHis expressed on three different promoters. From weakest to strongest, the following promoters were tested via both methods: ADH1, TEF, and GPD. The first method was to gather cell lysates of these constructs, along with an empty vector (EV) control, and perform an immunoblot with equal protein loading to monitor expression and to deduce sensor concentrations for each promoter using the calibration curve of known, purified HS1-monoHis. The second method was to use cells in a plate reader to read *in vivo* fluorescence values, as well as to read the fluorescence of purified HS1-monoHis in various concentrations to create a calibration curve. While the latter method was much easier to accomplish, the immunoblotting gave a much smaller sensor concentration – giving a range of sensor concentrations between 1.39 nM and 28.1 nM for the three different promoters. The fluorescence method produced concentrations between 3.60 μM and 29.4 μM, about 1000 times more concentrated than found by immunoblot. The fluorescence method operates under the assumption that the sensor behaves the same *in vivo*, like the different promoters in yeast cells, as it does *in vitro*, like the pure HS1-monoHis standards. Due to the smaller concentrations of the immunoblotting method, it was concluded that immunoblotting should be used in future tests of cellular sensor levels.

2.4.1 Fluorescence Method

In order to perform the fluorescence experiment, yeast cells were grown in Synthetic Complete-Leu (SC-Leu) medium. The following day, 10 OD/mL of cells were

collected, washed with water, and resuspended in 400 μL Phosphate-buffered saline

(PBS). At this point, 100 μL of each construct was loaded into wells on a black-bottom

fluoroplate alongside purified HS1-monoHis. The fluorescence of these cells was

measured for both eGFP (excitation:480 nm, emission:510 nm) and mKATE2

(excitation:580 nm, emission:620 nm). The concentrations of HS1-monoHis calculated

from this experiment can be seen in Table 1.

2.4.2 Immunoblotting Method

In order to perform the immunoblot, yeast cells were lysed using zirconium oxide

beads and a bullet blender. Lysate (20 μg) was then loaded onto a 12% tris tricine gel

along with four standard concentrations of purified HS1-monoHis (C1-C4) to create a

calibration curve. Once the gel was run, it was transferred onto a nitrocellulose

membrane and blotted with α-GFP antibody to quantify the amount of HS1-monoHis

present in each sample. As seen in Figure 13, the bands increase in intensity between the

different promoters according to their increase in expression strength. After

quantification of the bands, the concentrations of HS1-monoHis for each sample
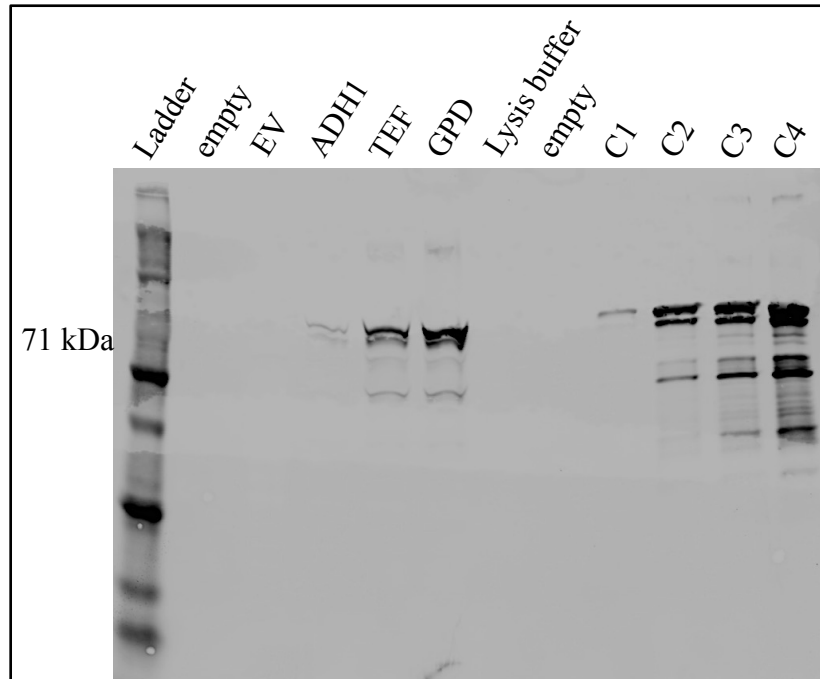
Figure 13. Immunoblot analysis to monitor HS1-monoHis levels in yeast cells with different strength promoters. Samples were resolved on a 10% tris glycine gel, transferred to a nitrocellulose membrane, and detected with commercially available antibodies. Lane 1: molecular weight marker. Lane 2: empty. Lanes 3-6: HS1-monoHis yeast cell lysates (20 µg) from increasing promoter strengths, EV, ADH1, TEF, and GPD. Lane 7: lysis buffer. Lane 8: empty. Lanes 9-12: purified HS1-monoHis in various concentrations to create a calibration curve.

were calculated using the calibration curve. The summary of sensor concentrations can be seen in Table 1. The large difference in the sensor concentrations, which vary by a factor of 10^3, indicated that the immunoblotting method was the most sensitive and reliable method to quantify sensor concentrations.

Table 1. HS1-monoHis concentrations calculated by immunoblotting and fluorescence

Construct	Western Blot (M)	Plate Reader (M)
ADH1	1.39×10^{-9}	3.60×10^{-6}
TEF	1.15×10^{-8}	1.44×10^{-5}
GPD	2.81×10^{-8}	2.94×10^{-5}

CHAPTER 3

IN CELL STUDIES OF VARIOUS HEME SENSORS

3.1 Introduction

To test the feasibility of these sensors *in vivo,* HS1, HS1-monoHis, and necessary

controls were transformed into *Saccharomyces cerevisiae,* or Baker's yeast. Yeast is an

ideal model organism because of its relative ease to work with; its entire genome is

sequenced and mapped, and it can easily be manipulated to grow with or without the

production of heme[35]. The halting of the production of heme is accomplished by

knocking out δ-aminolevulinic acid (ALA) synthase – the first enzyme in the biosynthetic

pathway – giving the hem1Δ cell line[36]. This genetic mutation can be overcome upon

addition of exogenous ALA, the next intermediate in the heme biosynthetic pathway.

Yeast cells in both wild type (WT) and hem1Δ cells were transformed with the various

heme sensors.

3.2 Fluorescence Test of HS1 and Controls

Once all sensor mutants were transformed into both WT and hem1Δ cell lines,

they were tested for the fluorescence of both chromophores. The first set of controls to be

tested was eGFP, mKATE2, and the mKATE2-eGFP fusion. These controls were created

to monitor the potential binding and quenching effects of heme to the chromophores

without the presence of a strong heme-binding motif, like cyt b_{562}. To this end, cells were

grown in SC-Leu medium were treated with ergosterol and Tween-80 to support growth

for hem1Δ cells (SCE-Leu medium). Hem1Δ cells have difficulty growing due to their

lack of ability to synthesize heme, which is vital in aerobic growth[36]. There was also a set

of hem1Δ cells that were grown with ALA supplementation at a concentration to support

WT levels of intracellular heme. This set of cells served as a control to show the ability of

cells to be rescued with ALA and to account for any peripheral effects on fluorescence

from knocking out ALA synthase when compared to WT cells.

The following mutants in hem1Δ cells were grown in SCE-Leu medium and half

were supplemented with 200 ng/μL ALA: HS1, eGFP, mKATE2, mKATE2-eGFP

fusion, and EV. The following day, 5 OD_{600}/mL of yeast cells were collected for each

sample and were resuspended in 1 mL phosphate-buffered saline (PBS). The fluorescence
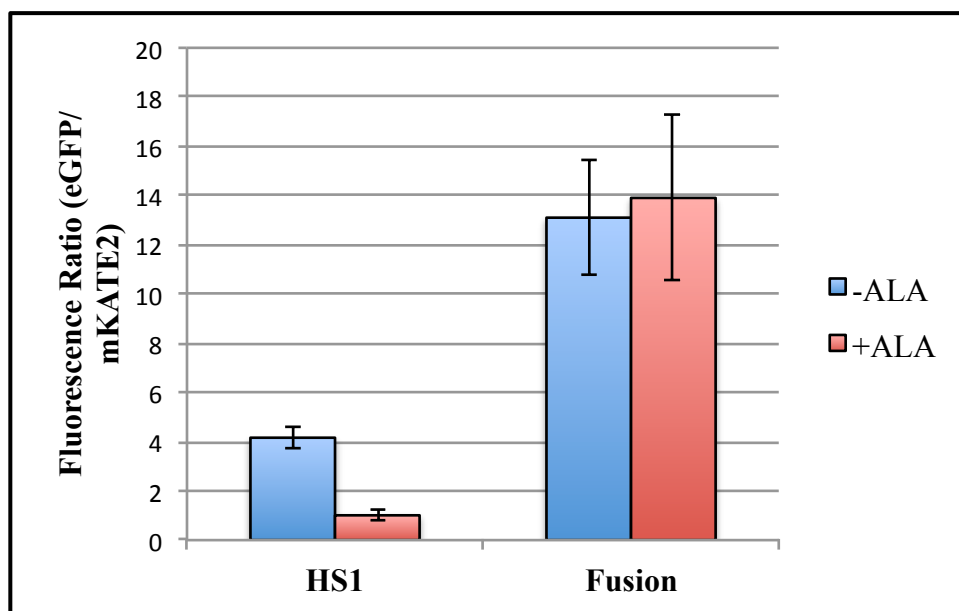
Figure 14. Fluorescence ratio in response to the presence of heme. HS1 and mKATE-eGFP fusion in hem1Δ yeast cells were inoculated without ALA (-ALA, blue bars) or supplemented with 200 ng/μL ALA (+ALA, red bars). After 15 hours of growth cells were added to a black-bottom fluoroplate and the eGFP fluorescence (excitation: 480 nm, emission: 510 nm) and mKATE fluorescence (excitation: 580 nm, emission: 620 nm) were measured. The ratio of eGFP:mKATE2 fluorescence was taken and is depicted above. An increase in heme concentration resulted in a decrease in eGFP fluorescence, resulting in a decrease in fluorescence ratio. The mKATE2-eGFP fusion was shown not to respond to heme because of its lack of heme-binding domain.

of these cells was then read by the plate reader after adding 100 μL of cells to each well in a black-bottom fluoroplate. As seen in Figure 14, the fluorescence ratios of the two chromophore-containing sensor constructs responded differently to the presence of heme. Due to the ability of eGFP to have energy transfer with heme, we would expect the fluorescence ratio to decrease in HS1 upon heme binding. The fusion control, mKATE2-eGFP, should not be affected by the presence of heme because of its lack of a heme-binding region. As seen in Figure 14, there was quenching of eGFP fluorescence, thereby reducing the HS1 ratio, when cells were supplemented with ALA to produce heme. It can

also be seen that the Fusion control was insensitive to the presence of heme, confirming the need for cyt b_{562} to facilitate FRET. It can thus be concluded that our HS1 sensor has a specific response to heme binding due to the presence of cyt b_{562} and not due to a peripheral binding event to one or both of the chromophores.

To extrapolate heme concentrations from fluorescence readouts, we need to know what value the fluorescence ratio of a 0% bound heme sensor looks like, as well as a 100% bound sensor fluorescence ratio. This can be achieved via an *in situ* calibration of the sensors. This procedure was optimized using a detergent, digitonin, which permeabilized the plasma membrane to allow extracellular heme into the cells to saturate the sensor-binding motif, giving a fluorescence reading corresponding to 100% bound[37].

The same cells tested in Figure 14 were pelleted and resuspended in 400 μL of a PBS solution with 50 μg/mL digitonin. These cells were incubated at 30 °C for 30 minutes to maximize permeabilization of the cell membranes. The PBS-digitonin solution was then removed, the cells were resuspended in 400 μL PBS, and the fluorescence was measured following the same conditions as the initial reading. One key difference from the initial fluorescence protocol above was the addition of a +/- heme condition to fully saturate the sensor after permeabilization. To the black-bottom fluoroplate 1 μL hemin chloride (1 mg/mL) solution was added to half of the wells to create the +heme condition. The other half of the plate was left without heme to give the –heme condition. As seen in Figure 15, HS1 was fully quenched upon heme addition following permeabilization. The HS1 fluorescence ratio shows a negative value for the +ALA+heme sample because it was quenched to below cellular background fluorescence. The blue bar for HS1 shows the ratio for what should be a 0% bound sensor due to its lack of ALA and heme, while

31
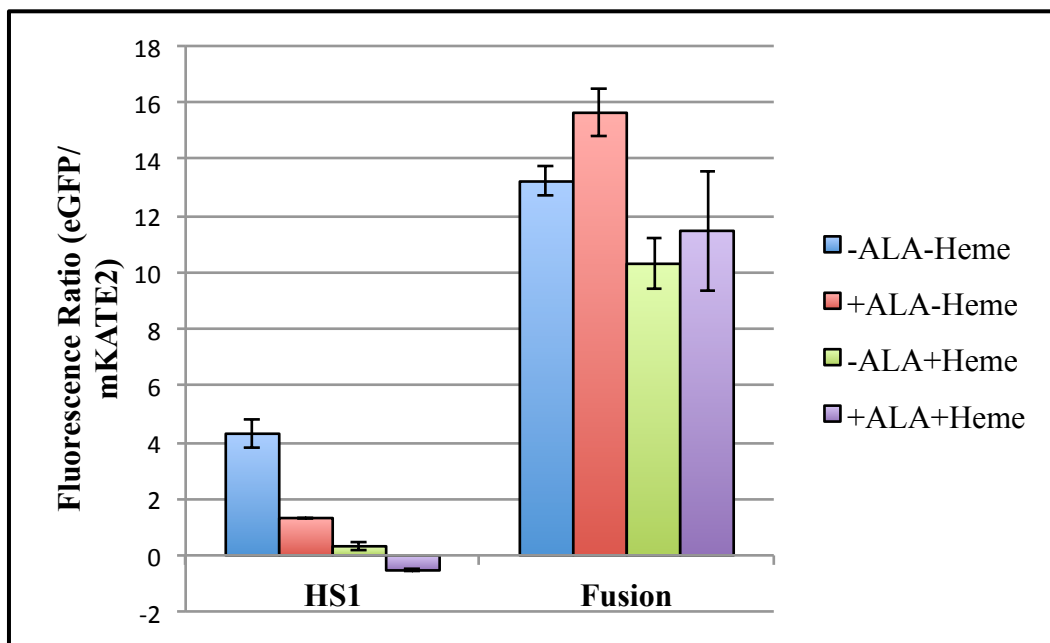
Figure 15. *In situ* calibration of HS1 and Fusion control. HS1 and mKATE-eGFP fusion in hem1Δ yeast cells were inoculated without ALA (-ALA) or supplemented with 200 ng/μL ALA (+ALA). After 15 hours of growth cells were permeabilized with 50 μg/mL digitonin for 30 minutes and added to a black-bottom fluoroplate both with 1 mg/mL heme (+Heme) and without heme (-Heme) and the eGFP fluorescence (excitation: 480 nm, emission: 510 nm) and mKATE fluorescence (excitation: 580 nm, emission: 620 nm) were measured. The ratio of eGFP:mKATE2 fluorescence was taken and is depicted above. An increase in heme concentration resulted in a decrease in eGFP fluorescence, resulting in a decrease in fluorescence ratio. The mKATE2-eGFP fusion was shown not to respond to heme because of its lack of heme-binding domain.

the purple bar shows the ratio for 100% bound. It should also be noted that the mKATE2-

eGFP fusion sensor was relatively unperturbed by the addition of ALA and heme. This

yet again supports that the heme-binding domain is the only contributor to FRET

exchange between heme and eGFP. This test was successful in laying the groundwork to

show that HS1 responds uniquely to heme, as well as to optimize digitonin

permeabilization and heme addition to achieve saturation of the sensor.

A screen of sensor fluorescence was also performed with HS1, HS1-monoHis, and EV yeast cells to see the *in vivo* response of HS1-monoHis to heme compared to that of HS1. The three different sensor variants in yeast cells were inoculated for both WT and hem1Δ into SCE-Leu medium. The hem1Δ mutants were both supplemented with 200 ng/μL ALA for heme production, as well as without ALA to give a zero heme background. After allowing them to grow overnight, cells were collected and resuspended in 1 mL PBS and the initial fluorescence was read for each of these constructs. Figure 16 shows the response of each sensor to the presence of ALA-supported heme and no heme. As seen in Figure 16, +ALA HS1 is essentially entirely quenched, further confirming the need for a weaker-binding sensor to expand our dynamic range. HS1-monoHis shows that weaker-binding property by having a +ALA fluorescence ratio of 6.1, compared to that of essentially 0 for HS1. This screen shows proof of principle for the use of these sensors *in vivo*, as well as the benefits of creating a larger library of mutants to give different heme binding affinities.
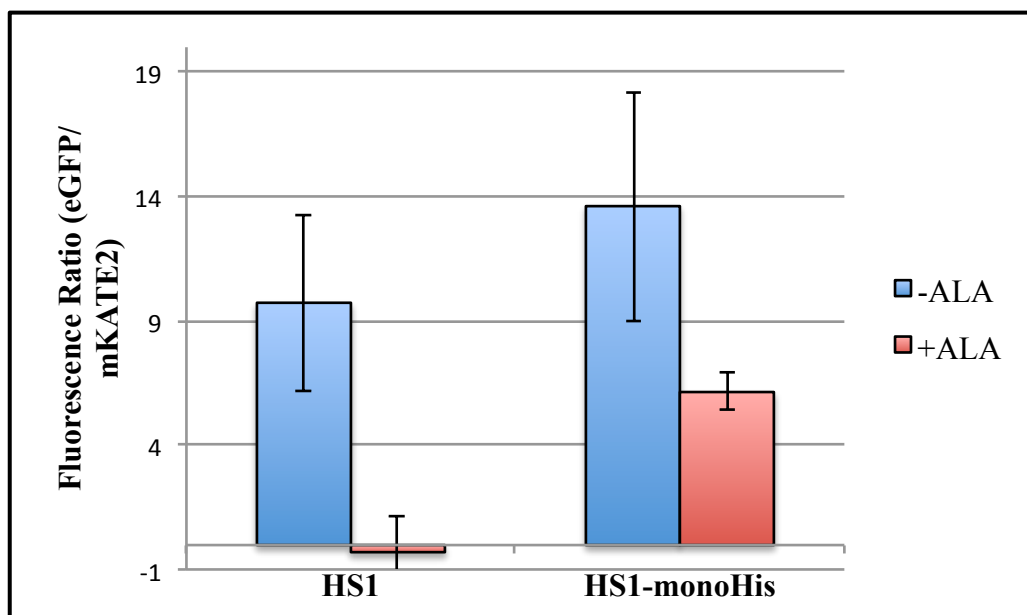
Figure 16. Fluorescence ratios of HS1 and HS1-monoHis in hem1Δ yeast cells. HS1 and HS1-monoHis in hem1Δ yeast cells were inoculated without ALA (-ALA, blue bars) or supplemented with 200 ng/μL ALA (+ALA, red bars). After 15 hours of growth cells were added to a black-bottom fluoroplate and the eGFP fluorescence (excitation: 480 nm, emission: 510 nm) and mKATE fluorescence (excitation: 580 nm, emission: 620 nm) were measured. The ratio of eGFP:mKATE2 fluorescence was taken and is depicted above. An increase in heme concentration resulted in a decrease in eGFP fluorescence, resulting in a decrease in fluorescence ratio. HS1-monoHis was shown to have a weaker binding affinity for heme when compared to HS1.

3.3 Heme Availability as a Function of Growth Phase

Now that we have demonstrated the utility of HS1 and HS1-monoHis, we are poised to address different questions using our sensors. The first question addressed was whether heme availability changes as a function of growth phase. In yeast cells there are three different growth phases that can be related to their optical density: the lag phase, the exponential phase, and stationary phase. In the experiments done previously, cells were collected between the exponential and stationary phase, not diligently keeping growth phase constant between experiments. We set out to address whether or not fluorescence,

indicative of heme availability, was dependent on growth phase. To this end, both WT

and hem1Δ cells harboring HS1, HS1-monoHis, and EV were inoculated into SCE-Leu

medium and fluorescence was monitored for the early exponential phase ($OD_{600} = 1$) and

stationary phase ($OD_{600} = 5$).
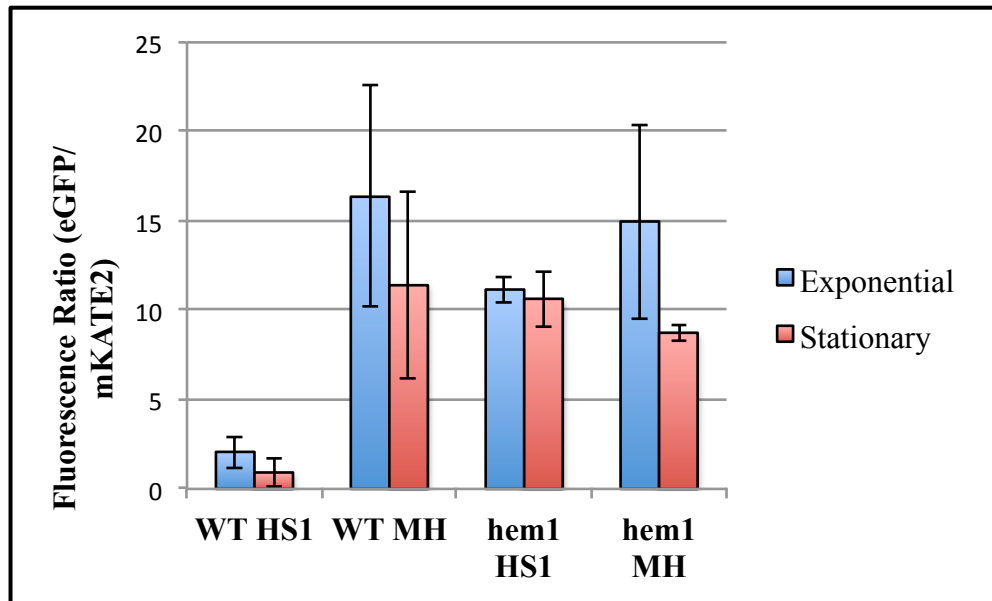
Figure 17. Heme availability as a factor of growth phase. HS1 and HS1-monoHis in WT
and hem1Δ (supplemented with 200 ng/ μL ALA)yeast cells were inoculated. After 15
hours (exponential, blue bars) and 24 hours (stationary, red bars) of growth, cells were
added to a black-bottom fluoroplate and the eGFP fluorescence (excitation: 480 nm,
emission: 510 nm) and mKATE fluorescence (excitation: 580 nm, emission: 620 nm)
were measured. The ratio of eGFP:mKATE2 fluorescence was taken and is depicted
above. An increase in heme concentration resulted in a decrease in eGFP fluorescence,
resulting in a decrease in fluorescence ratio.

The bars in Figure 17 do not show a reliable increase in cytosolic heme

concentrations because the results for both time points are within error of each other. This

result can be clarified better through repeating the experiment and taking more times points. For example, it would be nice to take samples from a variety of growth stages ranging from the lag phase ($OD_{600} = 0.5$) to the stationary phase ($OD_{600} = 5$), including more steps throughout the exponential phase, eg ($OD_{600} = 1, 3, 5, 7$). It has now been shown that our HS1 sensors can be used to determine different effects of heme in yeast cells.

CHAPTER 4

CONCLUSION AND FUTURE WORK

4.1 Conclusion

Heme is an important cofactor across various aspects of biology. Despite its ubiquitous nature in biology, relatively little is known about how heme is trafficked throughout the cell. To begin to understand this, a FRET-based heme sensor, HS1, was designed, purified, and expressed *in vivo*. HS1 was shown to be fully saturated with heme binding to cyt b_{562} in WT cells, so a different variant, HS1-monoHis, was created to have a weaker heme binding motif. This mutant was demonstrated to be less saturated with heme than HS1 in WT, but not devoid of heme as seen in the −ALA hem1Δ variant (Figure 16). In order to understand the concentration of our sensor as related to the pool of heme we're sensing, the concentrations of sensor in three different promoters were measured and were found to need further testing.

The sensors were expressed *in vivo* to show that they respond differently to different levels of heme upon ALA supplementation. As seen in the test of fluorescence as a result of growth phase, the sensors were able to detect different concentrations of heme available as a result of changing cellular environments. Our sensors have been validated to efficiently track heme changes in the cytosol and are now poised to answer more questions regarding heme biology in cells.

4.2 Future Work

Continued efforts are needed to expand the heme sensor library to create mutants that can cover a wider range of binding affinities, as well as design sensors that can selectively bind different oxidation states of heme. It would also be beneficial to create sensors that can be targeted to organelles known to require heme for their function, like the mitochondria and nucleus. This would allow the monitoring of heme movement to or from the cytosol in response to a stimulus, further uncovering the roles of heme in cell biology.

We would also benefit from the sensors being transfected into various mammalian cell lines representative of a number of diseases. Once a healthy cell line is reliably monitored, it would be helpful to compare the differences in heme availability in healthy cells to diseased cells. This can also be coupled to a genetic screen to elucidate the genes involved in regulating heme availability. These next steps are a few in a long line of necessary experiments needed to fully understand how heme functions throughout biology.

Table 2. Description of plasmids used

Plasmids Used	Description
pET30a(+)	Bacterial expression plasmid with N-terminal his_6-tag
pRH008	CG6 with his_6-tag at the N-terminus and TEV cleavage site
pRH013	HS1 with his_6-tag at the N-terminus and TEV cleavage site
pAR1023	HS1-monoHis with his_6-tag at the N-terminus and TEV cleavage site
pRH001	CG6 with his_6-tag at the N-terminus and thrombin cleavage site
pRH002	eGFP with his_6-tag at the N-terminus and thrombin cleavage site
pRH007	mKATE2-eGFP fusion with his_6-tag at the N-terminus and thrombin cleavage site

Table 3. Primers used for PCR reactions

Primers Used	Sequence
prRC004	GGTTCTGGATCCATGGTGTCCAAAGGTGAAGAACTG
prRC005	CAAGGTCAGTTTGCCAAAGGTAGCATCACC
prRC006	GGTGATGCTACCTTTGGCAAACTGACCTTG
prRC007	GGATATAAGCTTTCATTTATACAGTTCATCCATACCC
prRH008	GCAGATCTGGAAGACAACGCGGAAACTCTGAACG
prRH008-r	CGTTCAGAGTTTCCGCGTTGTCTTCCAGATCTGC

Expression and Purification of HS1. The gene encoding CG6 was digested with *Bam*HI and *Hind*III, ligated into pET30a(+) to give pRH008, and confirmed by sequence analysis. The gene encoding mKATE2 was then digested with *Bam*HI, ligated into pRH008 to give pRH013, and confirmed by sequence analysis. *Escherichia coli* BL21(DE3) containing pRH013 was incubated at 37 °C overnight in 20 mL Luria-Bertani medium supplemented with 50 μg/mL kanamycin. The next morning, 20 mL of the overnight culture was used to inoculate 1 L of Luria-Bertani medium supplemented with 50 μg/mL kanamycin. The resulting cultures were grown at 20 °C to an $OD_{600} = 0.8$ when protein expression was induced with the addition of 100 mM isopropyl β-D-thiogalactopyranoside (IPTG). Cultures were incubated at 20 °C for an additional 45 h. Harvested cells were resuspended in 30 mL of lysis buffer (20 mM Tris, 100 mM NaCl, pH 8.0, 1 mM PMSF, 1X ProteaseArrest™, 0.1X DNase). The cell membrane was disturbed using a French Pressure Cell Press (two passes on high at 1200 psi, 4 °C). The lysate was clarified by centrifugation (20000 rpm, 4 °C, 30 min). Total protein concentration was determined by the method of Bradford, using bovine serum albumin as a standard[38]. The cell-free extract was then loaded onto a 20 mL HisPrep FF 16/10 column prepacked with pre-charged Ni sepharose (GE Healthcare) with equilibration buffer (20 mM Tris, 100 mM NaCl, pH 8.0, 20 mM imidazole) to baseline as measured by UV-Vis. The HS1 protein was eluted by a gradient of 0 to 100% elution buffer (20 mM Tris, 100 mM NaCl, pH 8.0, 300 mM imidazole) over 15 column volumes, or 300 mL, collecting 10 mL fractions. Fractions containing the protein as confirmed via SDS-PAGE analysis were pooled and dialyzed against 3 L TEV cleavage buffer (20 mM Tris, 100 mM NaCl, pH 8.0) at 4 °C. The following day the his$_6$-tag was cleaved by adding a

1:1 molar ratio of TEV:HS1 and letting it incubate at room temperature for 18 h. Following incubation, the protein was loaded onto a 1 mL HisTrap HP column prepacked with pre-charged Ni sepharose (GE Healthcare) with equilibration buffer at 0.1 mL/min. Once all of the protein was loaded, the protein was eluted by increasing the flow rate to 1 mL/min, collecting 1 mL fractions. Upon elution, purity was checked via SDS-PAGE and was found to need further purification. The fractions containing HS1 were pooled and loaded onto a HiTrap Q HP 1 mL anion exchange column (GE Healthcare) with equilibration buffer (20 mM Tris, 10 mM NaCl, pH 8.0) at 0.1 mL/min. The column was washed with 5 column volumes of equilibration buffer at 1 mL/min and then equilibrated with 10% elution buffer (20 mM Tris, 1 M NaCl, pH 8.0). The protein was then eluted with a gradient of 10 to 25% elution buffer over 30 column volumes, or 30 mL, at a flow rate of 1 mL/min, collecting 300 μL fractions. Once purity was confirmed via SDS-PAGE, fractions were stored at 4 °C.

Expression and Purification of HS1-monoHis. The Met7 residue in cyt b_{562} was changed to Ala7 by a Quick Change polymerase chain reaction (PCR) using primers prRH008 and prRH008-r to give pAR1023. The product was confirmed by sequence analysis. *Escherichia coli* BL21(DE3) containing pAR1023 was incubated at 37 °C overnight in 20 mL Luria-Bertani medium supplemented with 50 μg/mL kanamycin. The next morning, 20 mL of the overnight culture was used to inoculate 1 L of Luria-Bertani medium supplemented with 50 μg/mL kanamycin. The resulting cultures were grown at 20 °C to an $OD_{600} = 0.8$ when protein expression was induced with the addition of 100 mM isopropyl β-D-thiogalactopyranoside (IPTG). Cultures were incubated at 20 °C for

an additional 45 h. Harvested cells were resuspended in 30 mL of lysis buffer (20 mM

Tris, 100 mM NaCl, pH 8.0, 1 mM PMSF, 1X ProteaseArrest™, 0.1X DNase). The cell

membrane was disturbed using a French Pressure Cell Press (two passes on high at 1200

psi, 4 °C). The lysate was clarified by centrifugation (20000 rpm, 4 °C, 30 min). Total

protein concentration was determined by the method of Bradford, using bovine serum

albumin as a standard[38]. The cell-free extract was then loaded onto a 20 mL HisPrep FF

16/10 column prepacked with pre-charged Ni sepharose (GE Healthcare) with

equilibration buffer (20 mM Tris, 100 mM NaCl, pH 8.0, 20 mM imidazole) to baseline

as measured by UV-Vis. The HS1-monoHis protein was eluted by gradient of 0 to 100%

elution buffer (20 mM Tris, 100 mM NaCl, pH 8.0, 300 mM imidazole) over 15 column

volumes, or 300 mL, collecting 10 mL fractions. Fractions containing the protein as

confirmed via SDS-PAGE were pooled and dialyzed against 3 L TEV cleavage buffer

(20 mM Tris, 100 mM NaCl, pH 8.0). The following day the his$_6$-tag was cleaved by

adding a 1:1 molar ratio of TEV:HS1-monoHis and letting it incubate at room

temperature for 18 h. Following incubation, the protein was loaded onto a 1 mL HisTrap

HP column prepacked with pre-charged Ni sepharose (GE Healthcare) with equilibration

buffer at 0.1 mL/min. Once all of the protein was loaded, the protein was eluted by

increasing the flow rate to 1 mL/min, collecting 1 mL fractions. Upon elution, purity was

checked via SDS-PAGE and was found to need further purification. The fractions

containing HS1-monoHis were pooled and loaded onto a HiTrap Q HP 1 mL cation

exchange column (GE Healthcare) with equilibration buffer (20 mM Tris, 10 mM NaCl,

pH 8.0) at 0.1 mL/min. The column was washed with 5 column volumes of equilibration

buffer at 1 mL/min and then equilibrated with 10% elution buffer (20 mM Tris, 1 M

NaCl, pH 8.0). The protein was then eluted with a gradient of 10 to 25% elution buffer over 30 column volumes, or 30 mL, at a flow rate of 1 mL/min, collecting 300 μL fractions. Once purity was confirmed via SDS-PAGE analysis, fractions were stored at 4 °C.

Expression and Purification of mKATE2-eGFP Fusion. The gene encoding cyt b_{562} was amplified out of the CG6 in pRH001 through two rounds of polymerase chain reaction (PCR) using primers prRC004, prRC005, prRC006, and prRC007. The product, pRH002, was confirmed by sequence analysis. The gene encoding mKATE2 was then digested with *Bam*HI, ligated into pRH002 to give pRH007, and confirmed by sequence analysis. *Escherichia coli* BL21(DE3) containing pRH007 was incubated at 37 °C overnight in 20 mL Luria-Bertani medium supplemented with 50 μg/mL kanamycin. The next morning, 20 mL of the overnight culture was used to inoculate 1 L of Luria-Bertani medium supplemented with 50 μg/mL kanamycin. The resulting cultures were grown at 25 °C to an $OD_{600} = 0.8$ when protein expression was induced with the addition of 100 mM isopropyl β-D-thiogalactopyranoside (IPTG). Cultures were incubated at 25 °C for an additional 24 h. Harvested cells were resuspended in 30 mL of lysis buffer (20 mM Tris, 100 mM NaCl, pH 8.0, 1 mM PMSF, 1X ProteaseArrest™, 0.1X DNase). The cell membrane was disturbed using a French Pressure Cell Press (two passes on high at 1200 psi, 4 °C). The lysate was clarified by centrifugation (20000 rpm, 4 °C, 30 min). Total protein concentration was determined by the method of Bradford, using bovine serum albumin as a standard[38]. The cell-free extract was then loaded onto a 20 mL HisPrep FF 16/10 column prepacked with pre-charged Ni sepharose (GE Healthcare) with

equilibration buffer (20 mM Tris, 100 mM NaCl, pH 8.0, 20 mM imidazole) to baseline

as measured by UV-Vis. The Fusion protein was eluted by gradient of 0 to 100% elution

buffer (20 mM Tris, 100 mM NaCl, pH 8.0, 300 mM imidazole) over 15 column

volumes, or 300 mL, collecting 10 mL fractions. Fractions containing the protein as

confirmed via SDS-PAGE were pooled and dialyzed against 3 L cleavage buffer (20 mM

Tris, 100 mM NaCl, pH 8.0) to remove imidazole. The following day the his$_6$-tag was

cleaved by adding a 1:10 dilution of thrombin (stock at a concentration of 50 units/μL)

and letting it incubate at room temperature for 15 h. Following incubation, the protein

was loaded onto a 1 mL HisTrap HP column prepacked with pre-charged Ni sepharose

(GE Healthcare) with equilibration buffer at 0.1 mL/min. Once all of the protein was

loaded, the protein was eluted by increasing the flow rate to 1 mL/min, collecting 1 mL

fractions. Upon elution, purity was checked via SDS-PAGE and was found to need

further purification. The fractions containing the Fusion were pooled and loaded onto a

HiTrap Q HP 1 mL anion exchange column (GE Healthcare) with equilibration buffer

(20 mM Tris, 10 mM NaCl, pH 8.0) at 0.1 mL/min. The column was washed with 5

column volumes of equilibration buffer at 1 mL/min and then equilibrated with 10%

elution buffer (20 mM Tris, 1 M NaCl, pH 8.0). The protein was then eluted with a

gradient of 10 to 25% elution buffer over 30 column volumes, or 30 mL, at a flow rate of

1 mL/min, collecting 300 μL fractions. Once purity was confirmed via SDS-PAGE,

fractions were stored at 4 °C.

REFERENCES

(1)   Auer, M.; Nicolussi, A.; Schutz, G.; Furtmuller, P. G.; Obinger, C. *J. Biol. Chem.* **2014**, *289*, 31480.

(2)   Yoshikawa, S.; Shimada, A. *Chem. Rev.* **2015**, *115*, 1936.

(3)   Severance, S.; Hamza, I. *Chem. Rev.* **2009**, *109*, 4596.

(4)   Mense, S. M.; Zhang, L. *Cell. Res.* **2006**, *16*, 681.

(5)   Que, L., Jr.; Tolman, W. B. *Nature* **2008**, *455*, 333.

(6)   Sono, M.; Roach, M. P.; Coulter, E. D.; Dawson, J. H. *Chem. Rev.* **1996**, *96*, 2841.

(7)   Dioum, E. M.; Rutter, J.; Tuckerman, J. R.; Gonzalez, G.; Gilles-Gonzalez, M. A.; McKnight, S. L. *Science* **2002**, *298*, 2385.

(8)   Lopez-Barneo, J. P., R.; & Ortega-Saenz, P. *Annu. Rev. Physiol.* **2001**, *63*, 259.

(9)   Kraut, H. P. a. J. *Science* **1992**, *258*, 1748.

(10)   Chiabrando, D.; Vinchi, F.; Fiorito, V.; Mercurio, S.; Tolosano, E. *Front. Pharmacol.* **2014**, *5*, 61.

(11)   Zitomer, R. S.; Lowry, C. V. *Microbiol. Rev.* **1992**, *56*, 1.

(12)   Batista-Nascimento, L.; Pimentel, C.; Menezes, R. A.; Rodrigues-Pousada, C. *Oxid. Med. Cell. Longev.* **2012**, *2012*, 128647.

(13)   Kumar, S.; Bandyopadhyay, U. *Toxicol. Lett.* **2005**, *157*, 175.

(14)   Jomova, K.; Vondrakova, D.; Lawson, M.; Valko, M. *Mol. Cell. Biochem.* **2010**, *345*, 91.

(15)   Pramanik, D.; Ghosh, C.; Dey, S. G. *J. Am. Chem. Soc.* **2011**, *133*, 15545.

(16)   Spiro, T. G. S., T. C. *J. Am. Chem. Soc.* **1973**, *96*, 338.

(17)   Wood, B. R.; Hammer, L.; Davis, L.; McNaughton, D. *J. Biomed. Opt.* **2005**, *10*, 14005.

(18)   Cupello, M. P.; Souza, C. F.; Buchensky, C.; Soares, J. B.; Laranja, G. A.; Coelho, M. G.; Cricco, J. A.; Paes, M. C. *Acta. Trop.* **2011**, *120*, 211.

(19) Luo, S.; Zhang, E.; Su, Y.; Cheng, T.; Shi, C. *Biomaterials* **2011**, *32*, 7127.

(20) Fahrni, C. J.; O'Halloran, T. V. *Journal of the American Chemical Society* **1999**, *121*, 11448.

(21) Domaille, D. W.; Que, E. L.; Chang, C. J. *Nature chemical biology* **2008**, *4*, 168.

(22) Shimomura, O. *J. Microsc.* **2005**, *217*, 1.

(23) Chalfie, M. T., Y.; Euskirchen, G.; Ward, W. W. & Prasher, D. C. *Science* **1994**, *263*, 802.

(24) Miyawaki, A. L., J.; Heim, R.; McCaffery, J. M.; Adams, J. A.; Ikura, M. & Tsien, R. Y. *Nature* **1997**, *388*, 882.

(25) Dittmer, P. J.; Miranda, J. G.; Gorski, J. A.; Palmer, A. E. *J. Biol. Chem.* **2009**, *284*, 16289.

(26) Miranda, J. G.; Weaver, A. L.; Qin, Y.; Park, J. G.; Stoddard, C. I.; Lin, M. Z.; Palmer, A. E. *PLoS One* **2012**, *7*, e49371.

(27) Arpino, J. A.; Czapinska, H.; Piasecka, A.; Edwards, W. R.; Barker, P.; Gajda, M. J.; Bochtler, M.; Jones, D. D. *J. Am. Chem. Soc.* **2012**, *134*, 13632.

(28) Jares-Erijman, E. A.; Jovin, T. M. *Nat. Biotechnol.* **2003**, *21*, 1387.

(29) Gisk, B.; Yasui, Y.; Kohchi, T.; Frankenberg-Dinkel, N. *Biochem. J.* **2010**, *425*, 425.

(30) Lezhneva, L.; Kuras, R.; Ephritikhine, G.; de Vitry, C. *J. Biol. Chem.* **2008**, *283*, 24608.

(31) Wang, Q.; Byrnes, L. J.; Shui, B.; Rohrig, U. F.; Singh, A.; Chudakov, D. M.; Lukyanov, S.; Zipfel, W. R.; Kotlikoff, M. I.; Sondermann, H. *PLoS One* **2011**, *6*, e23513.

(32) Gong, W.; Hao, B.; Mansy, S. S.; Gonzalez, G.; Gilles-Gonzalez, M. A.; Chan, M. K. *Proceedings of the National Academy of Sciences* **1998**, *95*, 15177.

(33) Nallamsetty, S.; Austin, B. P.; Penrose, K. J.; Waugh, D. S. *Protein Sci.* **2005**, *14*, 2964.

(34) Terpe, K. *Appl. Microbiol. Biotechnol.* **2003**, *60*, 523.

(35) Gollub, E. G.; Liu, K. P.; Dayan, J.; Adlersberg, M.; Sprinson, D. B. *J. Biol. Chem.* **1977**, *252*, 2846.

(36)   Atamna, H. *Ageing Res. Rev.* **2004**, *3*, 303.

(37)   Lemasters, J. J.; Holmuhamedov, E. *Biochim. Biophys. Acta.* **2006**, *1762*, 181.

(38)   Bradford, M. *Analytical Biochemistry* **1976**, *72*, 248.